

## ON THE USE OF VOLUMETRIC STRAIN METERS TO INFER ADDITIONAL CHARACTERISTICS OF SHORT-PERIOD SEISMIC RADIATION

BY R. D. BORCHERDT, M. J. S. JOHNSTON, AND G. GLASSMOYER

### ABSTRACT

Volumetric strain meters (Sacks-Evertson design) are installed at 15 sites along the San Andreas fault system, to monitor long-term strain changes for earthquake prediction. Deployment of portable broadband, high-resolution digital recorders (GEOS) at several of the sites extends the detection band for volumetric strain to periods shorter than  $5 \times 10^{-2}$  sec and permits the simultaneous observation of seismic radiation fields using conventional short-period pendulum seismometers. Simultaneous observations establish that the strain detection bandwidth extends from periods greater than  $10^7$  seconds to periods near  $5 \times 10^{-2}$  sec with a dynamic range exceeding 140 dB. Measurements of earth-strain noise for the period band,  $10^7$  to  $10^{-2}$  sec, show that ground noise, not instrument noise, currently limits the measurement of strain over a bandwidth of more than eight orders of magnitude in period. Comparison of the short-period portion of earth-strain, noise spectra ( $20$  to  $5 \times 10^{-2}$  sec) with average spectra determined from pendulum seismometers, suggest that observed noise is predominantly dilatational energy. Recordings of local and regional earthquakes indicate that dilatometers respond to  $P$  energy but not direct shear energy and that straingrams can be used to resolve superimposed reflected  $P$  and  $S$  waves for inference of wave characteristics not permitted by either sensor alone. Simultaneous measurements of incident  $P$ - and  $S$ -wave amplitudes are used to introduce a technique for single-station estimates of wave field inhomogeneity, free-surface reflection coefficients and local material  $P$  velocity. Estimates of these parameters derived for the North Palm Springs earthquake ( $M_w$  5.9) respectively for an incident  $P$  wave of  $29^\circ$  are  $-85^\circ$ , 1.71, 2.9 km/sec, and for an incident  $S$  wave of  $17^\circ$  are  $79^\circ$ , 0.85, 2.9 km/sec. The empirical estimates of reflection coefficients are consistent with model estimates derived using an anelastic half-space model with incident inhomogeneous wave fields.

### INTRODUCTION

Volumetric strain meters (Sacks *et al.*, 1971; Evertson, 1977) have been installed in boreholes at 15 sites along the San Andreas fault zone, California, to monitor long-period strain for earthquake prediction studies (Johnston *et al.*, 1982). Broadband, wide-dynamic range recorders (GEOS; Borchardt *et al.*, 1985) have been installed at several of these sites to extend the observation bandwidth for earth strain from periods of about 20 minutes to periods shorter than five hundredths of a second (Johnston and Borchardt, 1984). This extension in the short-period bandwidth was intended to permit the simultaneous observation of the radiation fields for a variety of sources including local, regional, and teleseismic earthquakes and to afford high-resolution measurements of pre- and co-seismic strain changes.

Benioff (1935) first pointed out that simultaneous observations of vectorial velocity and scalar strain permit inference of wave-field characteristics not permitted by either sensor alone. Motivated by observations from a vectorial pendulum seismograph and a linear strain meter, installed at the Seismological Laboratory, Pasadena, California, Benioff and Gutenberg (1952) utilized colocated measurements to infer characteristics of recorded surface waves. Romney (1957, 1959, 1964)

explained the advantages of combining linear strain and pendulum seismograph signals to improve the detectability of  $P$ . Gupta (1966) described the theoretical response of a vertical strain meter to body waves. Sacks *et al.* (1976) presented a formulation for single-site estimates of elastic phase velocity, using simultaneous measurements. More recently, with improvements in strain detection technology (see Agnew, 1986, for a comprehensive review), investigators have reported the observation of co-seismic strain offsets (McGarr *et al.*, 1982; Wyatt and Agnew, 1982; Johnston *et al.*, 1986, 1987a) and, with increasing frequency, volumetric strain perturbations for seismic radiation fields (Sacks *et al.*, 1971, 1978; Sacks, 1979; Snoke *et al.*, 1981; Suyehero, 1982; Johnston and Borchardt, 1984). However, the short-period response characteristics of volumetric strain meters, as installed *in situ*, have not yet been well established. In particular, the extent to which volumetric strain meters respond to dilatational energy but not shear energy and the extent to which the sensors might be utilized to resolve superimposed  $P$  and  $S$  wave fields for inference of wave characteristics not permitted by seismometers alone remains to be established. This paper is intended to serve as an initial examination of these questions.

Observations presented herein provide an estimate of earth-strain noise for periods ranging from  $10^7$  sec to  $5 \times 10^{-2}$  sec. The short-period portion of these spectra provide an estimate of detection thresholds for the radiation of volumetric strain signals as well as one of the initial estimates of short-period earth-strain noise.

Simultaneous observations of local and regional earthquakes demonstrate the short-period limits for the observation of volumetric strain perturbations as detected by installed sensors. They permit an examination of the extent to which dilatometers respond to dilatational radiation fields but not direct shear waves. They demonstrate the overlap in detection bandwidth for volumetric strain meters with that of short-period ( $f_0$ , 1 Hz) seismometers. The simultaneous measurements are used to introduce techniques for single-station estimates of incident wave field inhomogeneity, free-surface reflection coefficients, and local material velocity. Estimates, derived for incident inhomogeneous  $P$  and  $S$  waves, are compared to those predicted assuming incident homogeneous waves for both elastic and anelastic media. The estimates are derived using recent theoretical (Borchardt, 1988) and numerical (Borchardt and Glassmoyer, 1989) descriptions of body waves in a general viscoelastic half-space.

#### INSTRUMENTATION

Measurements of short-period dilatational strain and seismic particle velocity have been made for numerous regional and local events at several sites in California (Johnston and Borchardt, 1984). For this study we have chosen to concentrate on one of the more complete data sets recorded at a site in the Mojave Desert, California (Punchbowl, PUBS; Fig. 1).

Earthquakes recorded at the PUBS site are detected by three-component (1 Hz; L4 Mark Products) surface seismometers and a volumetric strain sensor cemented at a depth of 176 m in a borehole with expansive grout having density characteristics ( $2.3 \text{ gm/cm}^3$ ) similar to that of the host material. Signals from the sensors were recorded on site with broadband (0 to 600 Hz), wide dynamic range (156 dB), high-resolution (16-bit, 96 dB), portable, digital recorders. The volumetric strain signals were recorded at two gain levels at either 120 sps or 200 sps per channel with seven-pole Butterworth antialiasing filters chosen with high-cut corners at 33 or 50 Hz,

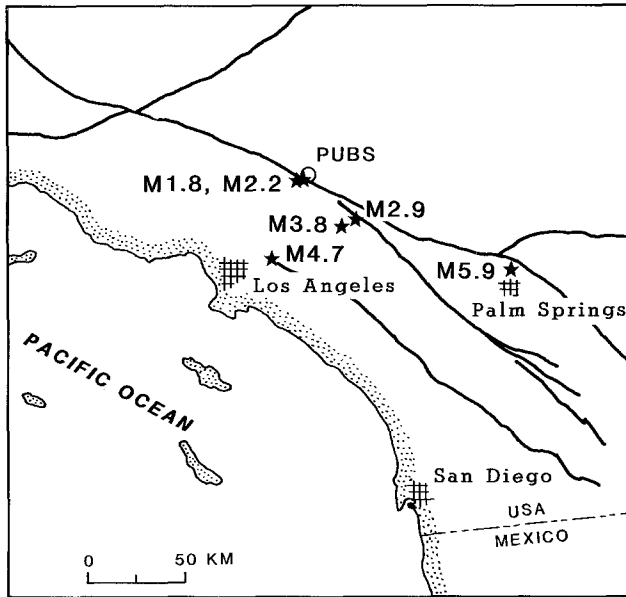


FIG. 1. Location of PUBS recording site in Mojave desert and epicenters of the earthquakes identified by magnitude (see Table 1).

respectively. A 50 Hz corner was used for the seismometer recordings (for a detailed description of the on-site recording system, GEOS, see Borchardt, *et al.*, 1985). In addition, signals from the dilatometer are recorded continuously via 16-bit, satellite telemetry at 1 sample per 10 minutes (Silverman *et al.*, 1988).

Calibration of the volumetric strain sensors and telemetry system at long periods is routinely provided to within an accuracy of about 5 per cent using ocean-load-corrected earth tides (Johnston *et al.*, 1982). Calibration of the seismometers and the GEOS unit is provided using signals generated by the field-recording unit. The *in situ* calibration signals are referenced to laboratory calibrations prior to deployment. Accuracy for the *in situ* seismometer calibrations is estimated to be within 2 per cent.

#### EARTH-STRAIN NOISE

Estimates of earth-strain noise specify a lower bound for direct observation of volumetric strain signals associated with earthquake radiation fields. An average estimate of earth-strain noise for the Punchbowl site is shown in Figure 2. This estimate was obtained over the period band ( $10^7$  to  $10^3$  sec) from satellite telemetry and over the period band ( $10^3$  to  $10^{-2}$  sec) with GEOS operating in continuous record mode.

The average earth-strain noise spectrum identifies the diurnal and semi-diurnal earth tidal periods and the microseismic peaks near 6 sec. The spectrum provides an estimate of earth-strain noise, interpreted not to be influenced by instrumentation noise levels, over the period band  $10^7$  to  $5 \times 10^{-2}$ . The spectrum suggests a bandwidth for observation of volumetric strain at earth-strain noise levels using the Sacks-Evertson dilatometer of more than eight orders of magnitude over a dynamic range greater than 140 dB. This bandwidth exceeds that of any currently available pendulum seismometer.

The short-period portion of the strain spectrum shows a decrease of about 10 dB

## AMBIENT NOISE ( EARTH STRAIN and GROUND VELOCITY )

PUNCHBOWL, CALIFORNIA

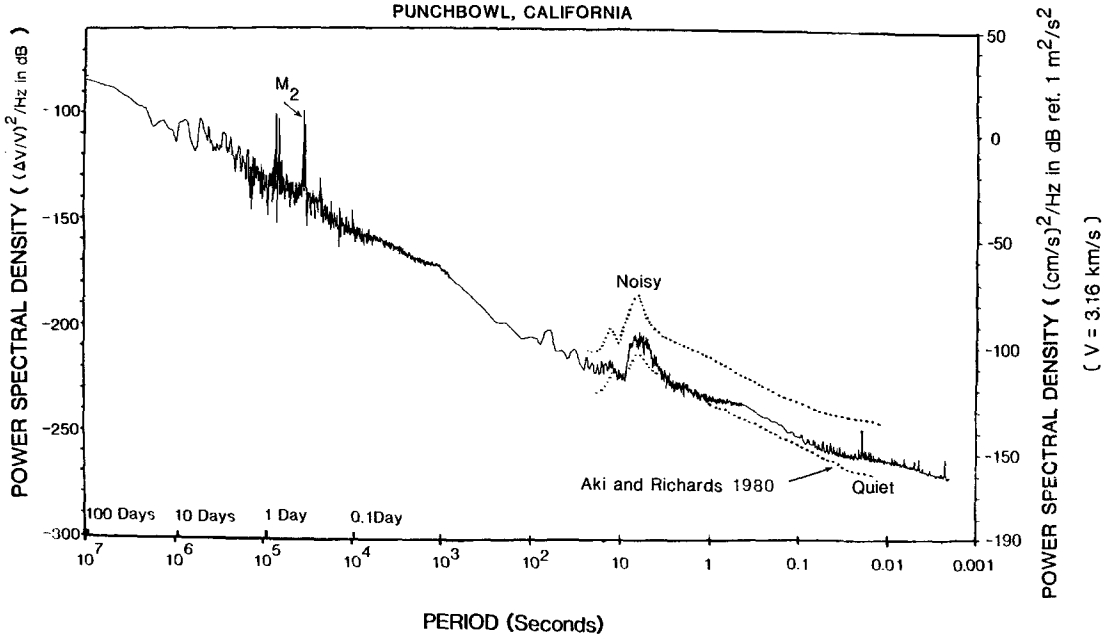


FIG. 2. Noise spectra derived from volumetric strain meter at site in Mojave desert, CA (PUBS) for the period band  $10^7$  to  $1.7 \times 10^{-3}$  sec. The spectra identify earth tidal and microseismic signals and earth-strain noise for period band  $10^7$  to  $5 \times 10^{-2}$  sec. Average spectra derived from pendulum seismometers (Aki and Richards, 1980) are provided for comparison.

per decade of period from  $-170$  dB (referenced to  $1 \epsilon^2/\text{Hz}$ ) at a period of  $10^3$  sec to  $-250$  dB near  $0.05$  sec. For comparison, an average spectrum for earth noise as determined from pendulum seismometers (Aki and Richards, 1980) is superimposed, assuming predominantly dilatational energy and reciprocal  $P$  velocity scaling ( $1/3.16$  km/sec; Borchardt, 1988). Similarity in the spectral shapes derived from the two types of sensors suggests that the observed noise is predominantly dilatational energy, probably associated with Rayleigh-type surface waves.

## STRAIN-METER RESPONSE TO SEISMIC RADIATION

As an example of the seismic radiation fields recorded at PUBS, the pendulum seismometer and volumetric strain time histories for the North Palm Springs event ( $M$  5.9, distance 134 km) are shown in Figure 3. The first trace shows the strain time history as recorded at 1 sample per 10 minutes for a 48-hr time period, which includes the occurrence of the event. Strain variations are evident due to earth tides, atmospheric pressure, and the strain offset of 17 nanostrain associated with the earthquake. (This offset interpreted with respect to a dislocation model yields a moment magnitude for the event of 6.0; Johnston *et al.*, 1987b.)

The volumetric strain and seismometer time histories recorded at high sampling rates (traces 2 through 5, Fig. 3) emphasize the long-period response capabilities of the dilatometer. The dominant energy on the dilatometer trace is in the 5- to 10-sec band, while that for the seismometer is near the sensors natural frequency (1 Hz).

Filtering the low-gain dilatometer trace with a high-pass filter (1 Hz; two-pole Butterworth) to approximate the low-frequency response of the seismometer shows

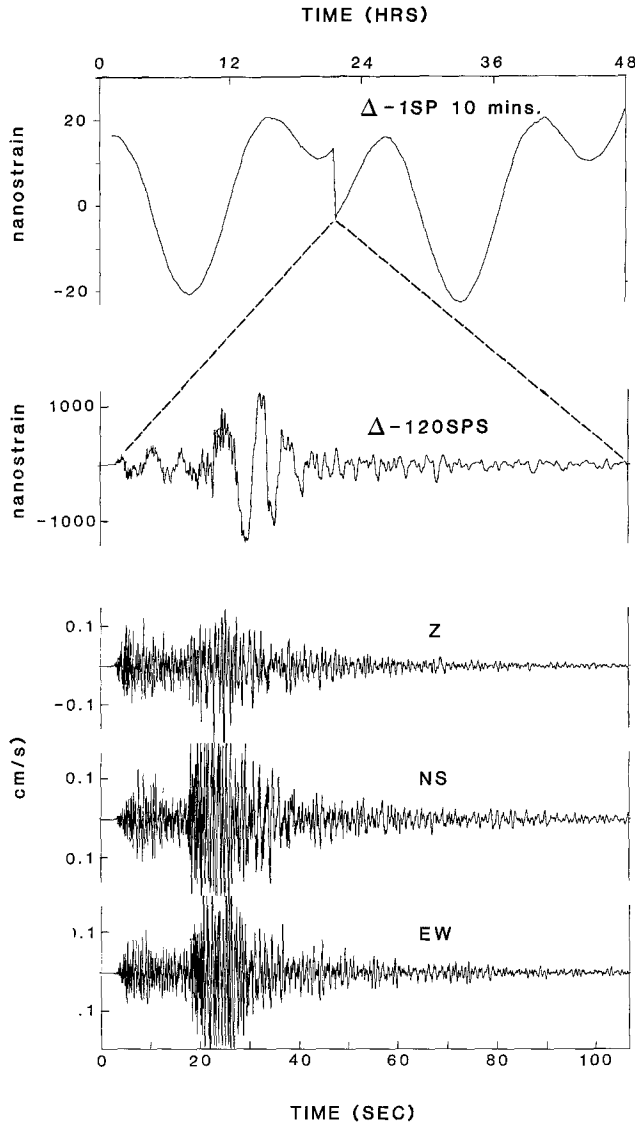


FIG. 3. Straingrams at two sampling sites (1 sp 10 mins. trace 1; 120 sps trace 2) and three-component seismograms signals (120 sps) recorded from the North Palm Springs earthquake at site PUBS. The strain time histories show tidal variations, a co-seismic strain offset (trace 1) and long-period seismic radiation (trace 2) not detected with short-period (1 Hz) seismometers.

that the dilatometer has substantial response to earthquake radiation above 1 Hz and in a short-period band common to the vertical seismometer (compare Fig. 4a with Fig. 4b). Application of a 20-sec high-cut filter to the dilatometer recording (Fig. 4c) reveals Rayleigh-wave energy at teleseismic periods. Expanded time histories, showing least-count noise levels, indicate detection levels near  $10^{-11}$  strain at 1 Hz (not shown).

To examine the capability of the volumetric strain meters to respond to short-period dilatational energy but not shear energy, we first provide a comparison of signals recorded during the initial part of the seismogram for which contamination by direct or converted *S* energy is considered less likely. The recordings for the North Palm Springs event are shown as originally recorded (Figs. 5a and 5c) and as bandpass-filtered between 2 and 8 Hz (Figs. 5b and 5d). The original dilatometer

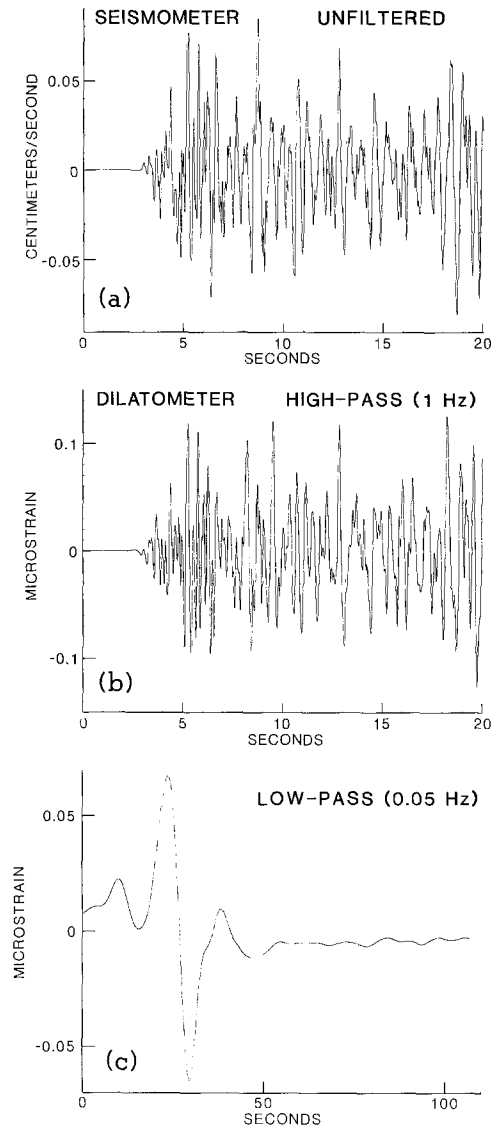


FIG. 4. Vertical seismogram and filtered straingrams signals recorded at PUBS during the North Palm Springs earthquake. The highpass-filtered (1 Hz; 2-pole) dilatometer signal indicates high-frequency seismic radiation in a passband common to that of short-period seismometer. Lowpass-filtered (0.05 Hz; 2-pole) signal demonstrates the response of the volumetric strain meter to seismic radiation outside the passband of short-period networks and conventional strong-motion recorders.

recording (Fig. 5a) provides evidence of long-period energy not apparent in the recording from the seismometer (Fig. 5c). Comparison of the bandpassed signals (Figs. 5b and 5d) shows that, in a pass band common to the two types of sensors, the shapes of the initial pulses are similar with only slight differences apparent in relative amplitudes near 5.3 sec.

Jones *et al.* (1986) used a velocity model introduced by Hadley and Kanamori (1978) to locate and determine focal mechanisms for the North Palm Springs event and its aftershocks. This model is comprised of three crustal layers extending to depths of 5.5, 16, and 32 km with corresponding  $P$  velocities of 5.5, 6.2, and 6.7 km/sec and a  $P_n$  velocity of 7.8 km/sec. Synthetic record sections, based on asymptotic raytracing with this model, using a formulation by Spence *et al.* (1984),

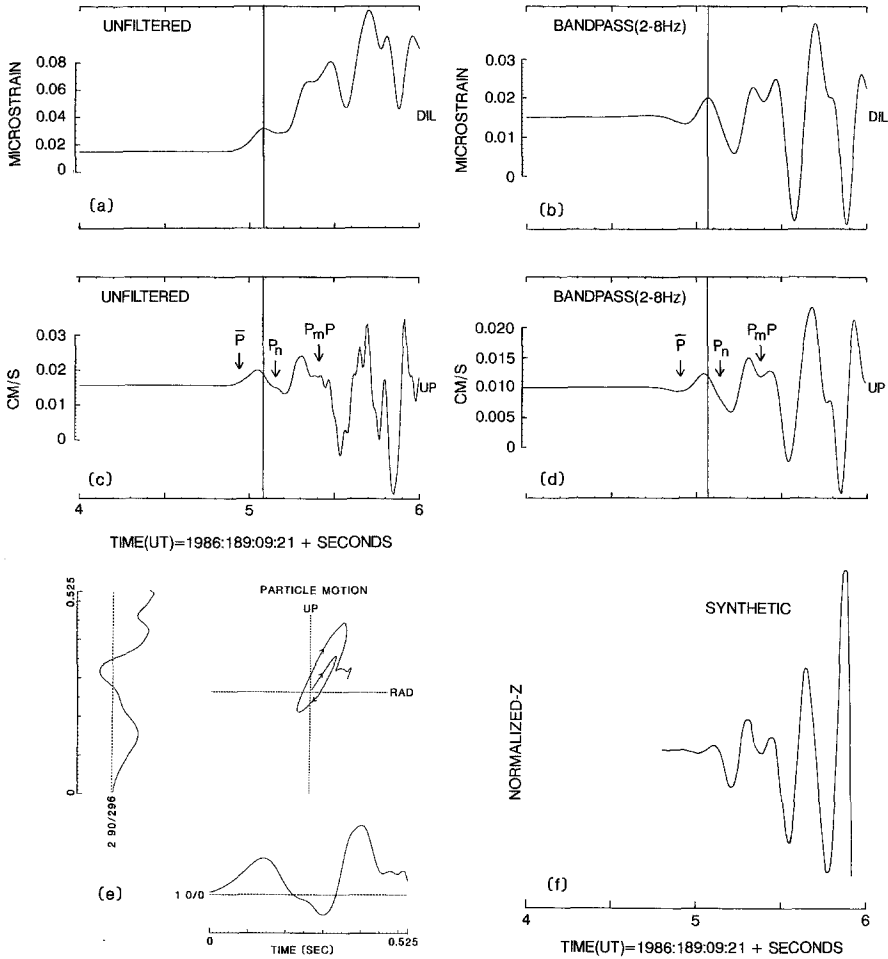


FIG. 5. Original (a, c) and bandpass-filtered (b, d), straingrams and vertical seismograms for  $\bar{P}$ ,  $P_n$ , and  $P_mP$  arrivals recorded from the North Palm Springs earthquake at PUBS together with corresponding synthetic seismograms (f) and observed particle motion (e).

as adopted for the PC by Crossley (1987), suggests that the successive arrivals at the PUBS site for the North Palm Springs event are  $\bar{P}$ ,  $P_n$ ,  $P_mP$ , and  $P-P$  within a time interval of about 2.0 sec (Figs. 5c, d). Comparison of the synthetic computed for the vertical seismometer (Fig. 5f) with that observed at a distance of 134 km (Fig. 5d) shows that the first second of the synthetic is in general agreement with that observed, both in relative amplitudes and travel times. This consistency between the synthetic and observed seismograms indicates that the first second of the North Palm Springs seismogram is dominated by dilatational energy associated with the identified arrivals. Consequently, the initial portion of the bandpassed vertical seismometer signal should be expected to correspond to a scaled version of the volumetric strain signal (Borcherdt, 1988). Similarity in the observed signals is consistent with this expectation and implies that the volumetric sensor is responding appropriately to the incident  $P$ -wave energy.

To further examine the capability of the dilatometer to discriminate between dilatational and shear energy, it is instructive to examine superimposed strain and seismometer signals recorded during both the arrival of  $P$  waves and  $S$  waves.

Superimposed plots for a local event ( $M_w$  1.8; distance 8 km, Fig. 6) and an earthquake near San Bernardino, California ( $M_w$  3.8; distance 48 km, Fig. 7) are typical of those obtained for other events. The time histories are bandpassed (2 to 6 Hz) to facilitate comparison in a frequency band common to the two types of sensors. Particle motion diagrams, computed from the original unfiltered recordings, provide an estimate of angle of incidence for  $P$  and  $S$  waves.

Comparison of the superimposed plots (Figs. 6 and 7) re-emphasizes that during the initial  $P$ -wave arrival, the pulses recorded on the two sensors are extremely similar. The pulses are displaced in time because of the spatial separation of the sensors. Comparison of the signals during the  $P$  coda, prior to arrival of the  $S$  wave, also shows considerable similarity in the dominant signals detected by the two types of sensors. Discrepancies in the smaller amplitude signals suggest arrival of con-

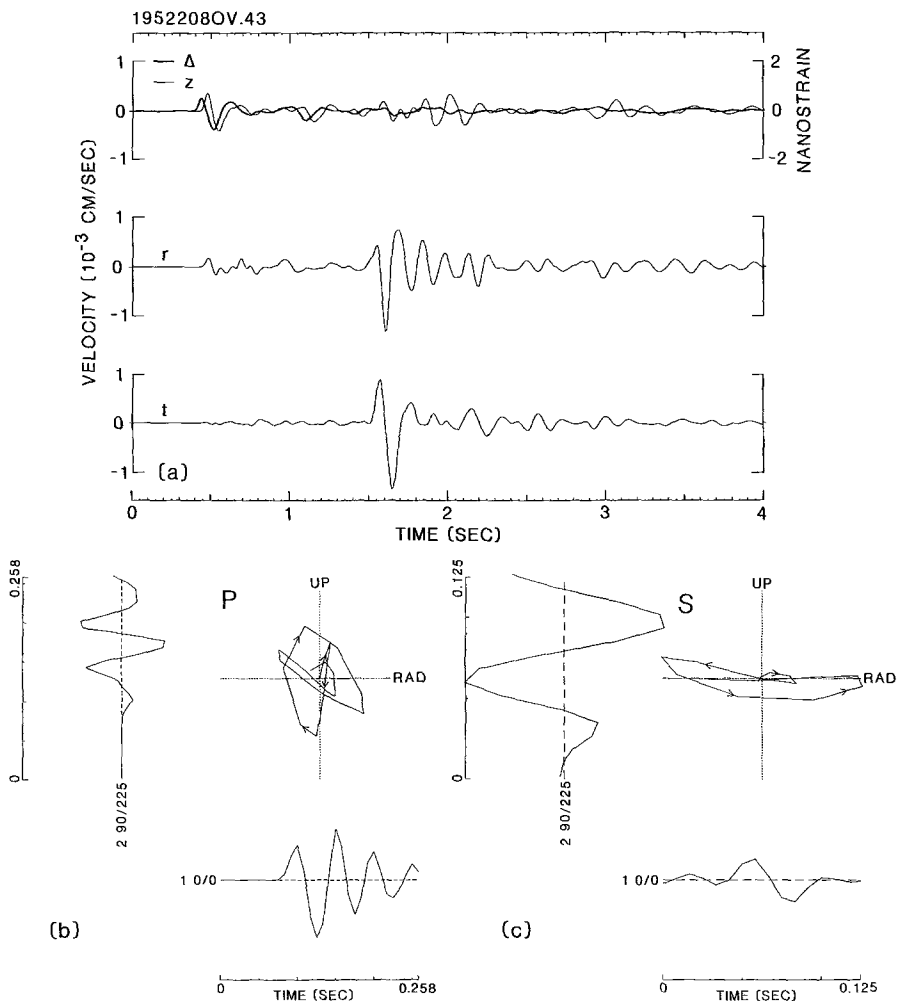


FIG. 6. Bandpassed (2 to 6 Hz) dilatometer ( $\Delta$ ), and seismometer signals ( $z$ ,  $r$ ,  $t$ ) recorded for a small ( $M_w < 2.0$ ) local earthquake at a distance of about 8 km from site PUBS. Similarity in pulse shapes for  $P$  arrival and lack of response during  $S$  arrival provides evidence that volumetric strain meter is responding to dilatational energy but not shear energy. Particle motions computed from unfiltered high-frequency  $P$  (b) and  $S$  (c) arrivals indicate angles of incidence for initial arrivals.

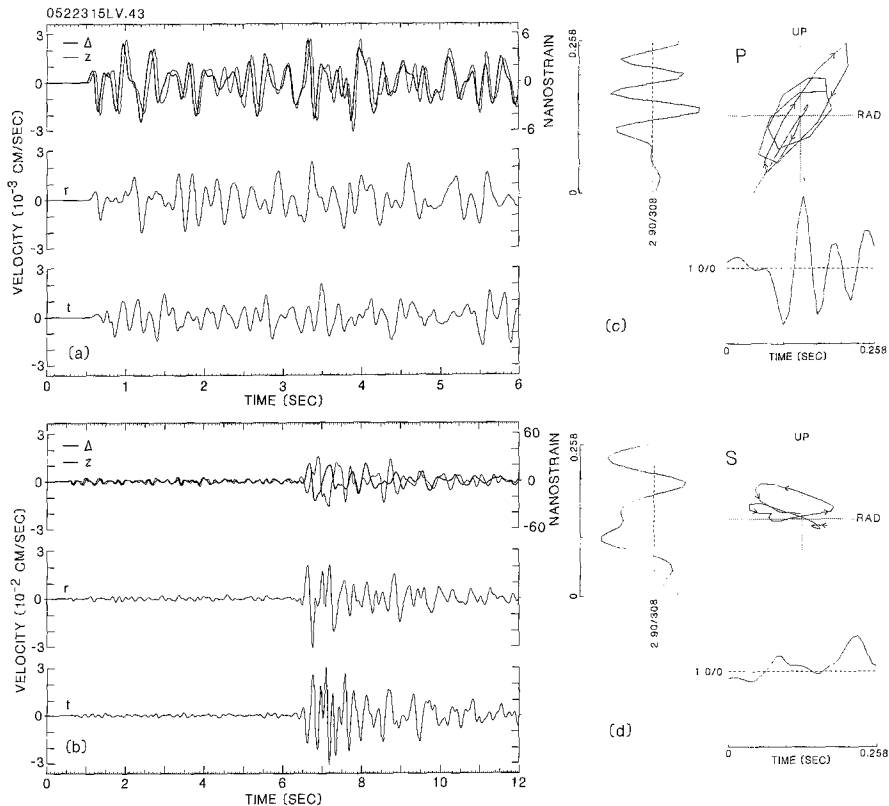


FIG. 7. Dilatometer ( $\Delta$ ) and three-component seismometer signals ( $z$ ,  $r$ ,  $t$ ) recorded for the San Bernardino event ( $M_w$  3.8, distance 48 km) at 120 sps at the PUBS site (*a*, *b*). Similarity in the superimposed dilatometer and vertical seismometer traces during the *P* coda (*a*, *b*) and dissimilarity during the *S* arrival (*b*) provides additional evidence that the dilatometer is responding predominantly to dilatational energy and only that shear energy converted to dilatational energy by the free surface. Estimates of free-surface reflection coefficients for incident *P* and *S* pulses using measured straingram and seismogram amplitudes are consistent with model estimates (see text) derived using angles of incidence and incident wave-field inhomogeneity inferred from particle motion diagrams (*c*, *d*).

verted energy. The similarity in the signals argues that the predominant energy arriving prior to the *S* wave is dilatational energy and not converted *P* to *S* energy.

Comparison of the superimposed plots (Figs. 6 and 7) during the *S* arrival shows significant differences in the signals detected by the two types of sensors. These differences are consistent with the dilatometer responding to only that *S* energy converted by the free surface to dilatational energy. The superimposed plots indicate that the dilatometer shows little or no response at the *S*-wave arrival time for the local event but shows a well-defined response for the San Bernardino event. This difference in response is consistent with model predictions in that the amount of dilatational energy generated by an *S* wave is strongly dependent on angle of incidence (Borcherdt and Glassmoyer, 1989).

Comparison of straingrams and seismograms for several other events shows similar results. These comparisons imply that the strain meters are responding primarily to dilatational energy. Little or no evidence has been found that they respond to incident *S* energy other than that converted to dilatational energy by the free surface. These preliminary results suggest that the volumetric strain meter provides a promising tool to resolve superimposed short-period *P* and *S* energy, when used in conjunction with colocated seismometers.

## SINGLE-STATION ESTIMATES OF WAVE-FIELD CHARACTERISTICS

Recordings at the PUBS site imply that the volumetric strain meter is responding predominantly to dilatational energy but not shear energy. Consequently, theoretical and numerical considerations (Benioff, 1935; Gupta, 1966; Borchardt, 1982; Borchardt and Glassmoyer, 1989) suggest that the simultaneous measurements should be useful for inferring wave characteristics not permitted by a pendulum seismometer alone. As examples, we utilize simultaneous measurements of strain- and velocity-component amplitudes to derive estimates of average local velocity and free-surface reflection coefficients.

Estimates of wave-field characteristics are compared with those derived from a half-space model using material parameters derived from a borehole log at a site displaced about 300 m from the dilatometer hole (Fumal, personal commun., 1988). This log yielded velocities of 3.55 and 1.94 km/sec for  $P$  and  $S$  waves at a depth of 110 m. Although velocities to the depth of the dilatometer (176 m) have not been measured, if we assume that the velocity at 176 km is the same as that at 110 m then average velocities computed for the site are 2.7 and 1.5 km/sec. If we also correct for a thin soil layer at the logging site but not the dilatometer site, we estimate the average velocities at the site to be 3.0 and 1.7 km/sec. An upper limit for intrinsic absorption values was adopted based on values measured for Pierre shale (McDonal *et al.*, 1958;  $Q_{HP}^{-1} = 0.03$ ;  $Q_{HS}^{-1} = 0.1$ ).

*The preferred half-space model adopted to predict the free-surface reflection coefficients accounts for inhomogeneity of the incident wave fields. Motivation to consider such a model is provided by the need to model the elliptical particle motions consistently observed for incident  $P$  and  $S$  waves. Calculations based on conventional elastic and anelastic models with incident homogeneous waves are provided for comparison. The model calculations are derived using a version of the code WAVES (Borchardt, 1988) adapted for a VAX. Detailed results of code predictions are presented in a companion paper by Borchardt and Glassmoyer (1989) and are not repeated here.*

*Incident  $P$* 

Particle motion diagrams, computed for several events, consistently show pronounced prograde elliptical motion for  $P$  waves (Figs. 5, 6, and 7). Ratios of the minor to major axis for six events ranging in distance from 8 to 134 km are tabulated (Table 1). For those events at distances greater than 40 km, the ratios for the initial pulses exceed 0.13 and for successive pulses (not shown) often approach unity indicating circular motion. (Particle motion loci, as reported herein, were computed using a technique based on orthogonalization of a matrix of cross-correlation functions described by Cranswick and Dietel, 1985).

An elastic plane wave model for an incident  $P$  wave does not account for the observed ellipticities. They predict linear particle motions for incident  $P$  waves inclined with respect to the vertical by an angle equal to twice that of the reflected  $S$  wave (Ben-Menahem and Singh, 1981, p. 93). Anisotropy also does not seem to be an explanation. Crampin (1984) concludes that any anisotropy in the earth is likely to have only a small effect on observations of seismic  $P$  waves.  $P$ -wave multipathing does not seem to be an explanation, because it seems unlikely that events with varying azimuths would yield consistent prograde particle motions especially during the arrival of the initial energy. The predominance of dilatational energy in the initial arrival as indicated by the dilatometer recordings argues against  $P$ - $S$  conversions below the dilatometer.

TABLE 1

SINGLE-STATION ESTIMATES OF ANGLE OF INCIDENCE ( $\theta$ ), INHOMOGENEITY ( $\gamma$ ), TOTAL VERTICAL FREE-SURFACE REFLECTION, AND AVERAGE LOCAL P VELOCITY FOR INCIDENT P WAVE USING SIMULTANEOUS MEASUREMENTS OF VOLUMETRIC STRAIN AND VERTICAL PARTICLE VELOCITY

Event	M	Distance (km)	Azimuth (degrees)	Apparent Angle (degrees)	Angle of Incident (degrees)	Minor/Major Axis	$\gamma$ (degrees)	$ \dot{\epsilon}_{z,z} $	$\dot{u}_{zz}/\Delta t$ km/sec/strain	$T_x$ observed	$T_x$ model	$\theta_{HP}$ observed	$T_{zP_1, P_2}$ inhomogeneous	$T_{zP_1, P_2}$ homogeneous	$T_{zP_1, P_2}$ Elastic
189	5.9	134	293	32	28	0.2	-85	1.02	5.13	1.7	1.71	2.9	0.65	0.58	0.58
052	3.8	48	304	33	29	0.16	-84	1.02	5.26	1.7	1.71	3.0	0.61	0.55	0.55
178	2.9	50	311	32	29	0.13	-82	1.01	5.70	1.9	1.71	3.3	0.60	0.58	0.58
195	1.8	8	225	24	21	0.07	-76	1.00	6.13	2.0	1.85	3.3	0.77	0.76	0.74
200	2.1	13	77	23	21	0.08	-77	1.00	6.00	2.0	1.85	3.2	0.77	0.76	0.76
042	4.7	46	22	29	25	0.18	-84	1.02	6.04	2.0	1.78	3.3	0.71	0.64	0.64

Another possible model for consideration is that of an anelastic half-space but with incident homogeneous waves. This model predicts that the reflected *S* wave is inhomogeneous and that the free-surface particle motions are elliptical (Borcherdt, 1982; Borcherdt and Glassmoyer, 1989). However, our calculations for an incident homogeneous *P* wave, indicate that departures from linearity for the free-surface particle motion due to the sum of the incident and reflected waves is an order of magnitude less than that observed, even with substantial variations in  $Q_{HP}^{-1}$  and  $Q_{HS}^{-1}$ . Consequently, we conclude that the half-space model most appropriate to account for the observed ellipticities in the initial *P* particle motion is that for which the incident wave fields are inhomogeneous.

Inhomogeneity of the incident wave fields is consistent with theoretical and numerical predictions for body waves in layered low-loss anelastic media (Borcherdt, 1973, 1977, 1982; Borcherdt and Wennerberg, 1985; Borcherdt *et al.*, 1986). It can be used to account for any degree of observed ellipticity, because particle motion loci tend toward circularity as the inhomogeneity of the wave field increases. Formulation of the model in terms of incident inhomogeneous waves allows results for the special case of incident homogeneous waves in either anelastic or elastic media to be readily deduced.

Straightforward measurements, derivable from the straingram and the seismograms, are the maximum amplitudes of the initial pulses. At the free surface, this amplitude on a vertical seismogram ( $\dot{u}_{RZ_{P_1, P_2, S_2}}$ ) represents the amplitude due to the sum of the incident *P* wave ( $p_1$ ) and the reflected *P* ( $p_2$ ) and *S* ( $s_2$ ) waves. At the depth of the dilatometer (176 m), this amplitude on the strain meter ( $\Delta_{R_{P_1}}$ ) is assumed to be that for the incident *P* wave. An expression for the vertical free-surface reflection coefficient ( $r_{z_t}$ ) that involves these measurements for an incident inhomogeneous *P* wave is

$$r_{z_t} \equiv \frac{u_{RZ_{P_1, P_2, S_2}}}{u_{R_{P_1}}} = \frac{\dot{u}_{RZ_{P_1, P_2, S_2}}}{\Delta_{R_{P_1}}} \cdot \frac{|k_p|}{\omega} \cdot \frac{1}{|\xi_{1_{P_1}}|} \tag{1}$$

where for low-loss solids the ratio ( $\omega/|k_p|$ ) of angular frequency to wave number modulus is approximately the *P*-wave velocity ( $v_{HP}$ ) and  $|\xi_{1_{P_1}}|$  represents the normalized length of the major axis of the incident particle motion ellipse (notation presented here is developed in detail; Borcherdt, 1988).  $|\xi_{1_{P_1}}|$  is unity for incident homogeneous waves.

Equation (1) shows that measurement of the ratio of maximum vertical velocity to maximum volumetric strain and knowledge of material parameters provide an estimate for the total vertical free-surface reflection coefficient. Conversely, independent estimates of the free-surface reflection coefficient as might be derived from a borehole seismometer or a model, suggests inference of local *P* velocity.

Apparent angles of incidence, as inferred from inclinations of the particle motion loci, were used to infer actual angles of incidence for the *P* arrivals (Table 1). These vary from 21 to 29 degrees. Measurements of the ratio of the minor to major axis were used to infer degrees of wave-field inhomogeneity (Table 1), which vary from -76 to -84 degrees. Total free-surface reflection coefficients implied by the model calculations ( $r_{z_t}$  model; Table 1) vary between 1.71 and 1.85. The inferred degrees of inhomogeneity imply that the incident wave fields propagate with a reduced velocity and greater attenuation than corresponding homogeneous waves. For example, the inhomogeneity inferred for the North Palm Springs event (189; -85°) implies the incident wave propagates at a velocity of 5 per cent less and a  $Q^{-1}$  25

per cent greater than a corresponding homogeneous  $P$  wave. These deviations are of sufficient size for measurement, but with an elastic model could easily be attributed to material variations.

Estimates of the ratio of peak velocity to volumetric strain ( $\dot{u}_{RZ_{P_1, P_2, S_2}}/\Delta_R$ : Table 1) were derived from peak-to-trough measurements for the first  $P$  pulse. These estimates when substituted into 1 yield estimates of the total vertical free-surface reflection coefficient ( $r_{z_t}$  obs; Table 1). These estimates vary between 1.7 and 2.0 km/sec/strain. They are in general agreement with those calculated by the model ( $r_{z_t}$  model). As a check on consistency of the results, we substituted the model estimate of the reflection coefficient ( $r_{z_t}$  model) and the measured velocity strain ratio ( $\dot{u}_{RZ_{P_1, P_2, S_2}}/\Delta_R$ ) into 1 to infer the local  $P$  velocity ( $v_{HP}$  obs; Table 1). The inferred velocities range between 2.9 and 3.3 km/sec. These estimates are considered consistent with the estimate of 2.98 km/sec implied by the nearby borehole log.

Estimates of the vertical reflection coefficient for the reflected  $P$  wave also are provided in Table 1. These estimates were computed for our preferred model with incident inhomogeneous waves and for corresponding elastic and anelastic models with incident homogeneous waves (Table 1). For the events considered the results for the elastic and anelastic models with incident homogeneous waves agree to within about 2 per cent. Those for the preferred model show deviations from these up to 11 per cent (compare last three columns, Table 1). In general, we find that deviations implied by the model increase with increasing angle of incidence and inhomogeneity. The size of the deviation depends on the wave characteristics of interest. The possibility for large deviations is consistent with laboratory results for low-loss anelastic media (Borcherdt *et al.*, 1986).

### *Incident S*

Particle motions computed for the  $S$  waves of the events recorded at PUBS also consistently show evidence for elliptical motions (e.g., see Figs. 6c and 7d). In general, however, the particle motions for  $S$  are more complicated than for  $P$ . The particle velocity locus, in general, appears to circumscribe an ellipsoidal figure with the plane and ellipticity of the locus often changing significantly as the locus progresses with time. In the case of  $S$  wave additional factors contribute to more complicated particle motions.

Elastic models do not account for the observed ellipticity, because they predict elliptical motion only for angles greater than critical (Nuttli, 1961; Mediguren, 1969). For the events considered here, the incident angles inferred for  $S$  waves are substantially less than critical.

Anisotropy also does not seem to account for observed ellipticity. Anisotropic models predict separation of  $S$  energy or  $S$  wave splitting (e.g., Crampin *et al.*, 1982; Peacock *et al.*, 1988). The models for transversely anisotropic media predict two quasi-shear waves for parallel layered models, each being linearly polarized perpendicular to the direction of phase propagation (Crampin, 1984). Superposition of these two quasi-shear-wave signals could lead to a variety of particle motions for the incident wave fields in a plane defined by the rectilinear polarizations. For the seismograms inspected, we found little evidence for rectilinear motion or planar motion.

Simultaneous or near simultaneous arrival of  $SV$  and  $SH$  energy serves to complicate particle motion loci compared during the initial  $S$  arrivals. This complication makes it difficult to infer the saggital plane or radial direction for arrival of  $SV$  energy, which because of lateral refraction may be different from that for the

initial  $P$  energy. The inability to refine the estimate of the radial direction can contribute to complications in inferred  $S$  particle motion.

The record from the volumetric strain sensor (Fig. 7) suggests that superimposed converted  $S$  to  $P$  energy below the dilatometer is probably not a major contributor to the observed ellipticity for initial  $S$  arrival; however, converted energy could be expected to contaminate particle motion diagrams for later arrivals.

For the problem of an incident  $S$  wave in the absence of superimposed incident  $P$  energy, the volumetric-strain signal should correspond to only that signal associated with the  $P$  wave reflected from the free surface. The signal from a surface seismometer should represent a superposition of those associated with the incident  $S$  wave and both types of reflected waves. Consequently, if this is the case, then the maximum vertical velocity can be determined from that recorded on the strain meter using

$$\dot{u}_{RZ_{P_2}} = v_{HP} F_{P_2}(\cos \theta) \cdot \Delta_{R_{P_2}}, \tag{2}$$

where  $F_{P_2}(\cos \theta_2)$  is the modulation factor for the reflected  $P$  wave and can be expressed in terms of that for the incident  $S$ -I wave (equation (8b) in Borchardt and Glassmoyer, 1989). Rewriting (2) in terms of the maximum vertical velocity measurable at the free surface ( $\dot{u}_{RZ_{S_1, P_2, S_2}}$ ) yields an expression for the vertical reflection coefficient for the reflected  $P$  wave, namely,

$$r_{zp} \equiv \frac{u_{RZ_{P_2}}}{u_{RZ_{S_1}}} \approx v_{HP} \cdot F_{P_2}(\cos \theta_{P_2}) \cdot \frac{u_{RZ_{S_1, P_2, S_2}}}{u_{R_{S_1}}} \cdot \frac{\Delta_{R_{P_2}}}{\dot{u}_{RZ_{S_1, P_2, S_2}}}. \tag{3}$$

Consequently, from measurements of the amplitude for volumetric strain and vertical velocity, we can use model calculations to infer the vertical reflection coefficient for the reflected  $P$  wave or, as a check on consistency, use model calculations to infer local  $P$  velocity. Similar expressions can be readily derived for the horizontal reflection coefficient using measurements of maximum radial velocity. We illustrate (3) using measurements from the San Bernardino event, whose recordings showed well-defined pulses for the initial  $S$  arrival.

The orientation of the major axis for the San Bernardino event implies an apparent angle of incidence for the  $SV$  wave of 21 degrees and an actual angle of incidence of about 17 degrees. As mentioned earlier, this angle of incidence is significantly less than the estimated critical angle of 35 degrees. For inhomogeneity to account for the observed ellipticity, the ratio of minor to major axis (0.26; Fig. 7d) implies that the degree of inhomogeneity for the incident wave is about  $\gamma = 79$  degrees. This degree of inhomogeneity implies that the velocity and  $Q$  for the incident wave are about 97 and 83 per cent, respectively, those for a corresponding characteristic wave in the medium (Borchardt and Wennerberg, 1985).

The inhomogeneity (79 degrees) and angle of incidence (17 degrees) inferred for the incident  $S$ -I wave imply that the reflection coefficient for the total motion at the free surface ( $u_{RZ_{S_1, P_2, S_2}}/u_{R_{S_1}}$ ) is 0.82 and  $F_{P_2}(\cos \theta_{P_2}) = 0.99$ . Measuring the amplitude of the first pulses observed on the strain meter and the vertical seismometer for the  $S$  wave yield  $\dot{u}_{RZ_{S_1, P_2, S_2}}/\Delta_{R_{P_2}} = 2.91$  km/sec/strain. Substitution of these numbers and an average  $P$  velocity of 2.98 km/sec implies that the vertical reflection coefficient for the reflected  $P$  wave is 0.83. This number agrees well with that (0.81) computed directly by the model. As a check on consistency, substitution of the computed reflection coefficients into (3) yields an estimate for local  $P$  velocity of 2.9 km/sec.

If we don't account for the observed elliptical particle motions and use an anelastic half-space model with incident homogeneous waves, then we find that model estimates of the reflection coefficients in (3) differ significantly from those just computed. Specifically, incident homogeneous waves and the same anelastic material parameters imply that the total reflection coefficient is 0.64,  $F_{P2}(\cos \theta_{P2}) = 0.85$ , and the vertical reflection coefficient for the reflected  $P$  wave is 0.53. (For comparison, our previous estimates with incident inhomogeneous waves yielded corresponding estimates of 0.82, 0.99, and 0.81.) An elastic model yields estimates essentially identical to those for the incident homogeneous anelastic model. Consequently, of the three half-space models, we prefer the one which accounts for the ellipticity observed for the incident waves.

### DISCUSSION

Recent improvements in the technology for the detection and recording of earth strain extends the observation band for volumetric strain from periods greater than  $10^7$  seconds to periods shorter than  $5 \times 10^{-2}$  sec over amplitudes ranging from  $10^{-6}$  to near  $10^{-11}$  strain at 1 Hz. These extensions in bandwidth and detection thresholds extend routine observation capabilities to periods ( $>15$  sec) not observable using short-period networks or strong-motion accelerometers. These extensions permit the routine observation of ultra long periods as well as short-period pre- and co-seismic strain changes at levels down to  $10^{-11}$  strain (Johnston *et al.*, 1986). The observation bandwidth for strain overlaps the period passbands and amplitude ranges for long- and short-period pendulum seismometers and accelerometers. These overlaps permit the simultaneous observation of scalar volumetric strain and inferred vectorial displacement fields for seismic events at teleseismic, regional and near-source distances over a dynamic range greater than 140 dB.

Simultaneous recordings of strain and three-component seismic velocity suggest that dilatometers detect, within uncertainties of present data sets, dilatational energy but not shear energy for seismic radiation at earth-noise levels for periods down to and including 0.05 sec. Straingrams of initial  $P$  energy represent, within uncertainties of present data, vertical seismograms, scaled by factors accounting for angle of incidence, local material parameters, and wave field inhomogeneity. Straingrams, during the arrival of  $S$ -wave energy, describe inhomogeneous  $P$  waves reflected from the free surface with amplitudes consistent with model predictions accounting for inhomogeneous anelastic wave fields. Spectra of earth-strain noise provide an estimate of detection thresholds for radiation of short-period volumetric strain.

Theoretical and numerical considerations (Benioff, 1935; Borchardt, 1988; Borchardt and Glassmoyer, 1989) suggest that strain meters might be utilized together with collocated seismometers to resolve superimposed  $P$  and  $S$  waves and, in turn, infer characteristics not permitted by either sensor alone. Measurements of straingram and vertical seismogram amplitudes for incident  $P$  and  $S$  waves provide single-station estimates of wave-field inhomogeneity, free-surface reflection coefficients, and local  $P$  velocities. Estimates of average  $P$  velocity at the site (2.9 to 3.3 km/sec) are consistent with an estimate (2.98 km/sec) derived from nearby borehole measurements. Estimates of free-surface reflection coefficients (Table 1) are consistent with model estimates computed for inhomogeneous  $P$  and  $S$ -I waves incident on the free surface of an anelastic half-space. This half-space model is preferred over either elastic or anelastic half-space models with incident homogeneous waves, because it accounts for the elliptical particle motions consistently observed for

incident  $P$  and  $S$  waves. Inferred degrees of inhomogeneity (see Table 1) imply measurable variations in velocity and  $Q^{-1}$  for the incident waves, but variations that are not so large as to be inconsistent with material variations to which they might be attributed if a model assuming linear particle motions were used.

The influence of wave inhomogeneity is well known in those cases predicted to exist by elasticity. Two familiar cases are those of waves refracted beyond their critical angle and Rayleigh waves. In both of these cases, the resultant particle motions are predicted to be elliptical with the degree of inhomogeneity for the component solutions being 90 degrees. Nuttli (1961) provided an account of observed elliptical motions for  $SV$  waves incident at angles beyond critical using an elastic model. His solutions for the critically refracted  $P$  waves were those describing an inhomogeneous  $P$  wave with phase propagation parallel and maximum attenuation perpendicular to the free surface. Introduction of anelasticity implies that in addition to these cases, body waves having traversed any change in anelastic material properties will, in general, be inhomogeneous. Consequently, while the predominant type of body wave expected on the basis of layered elastic models is homogeneous, the predominant type expected on the basis of anelastic models is inhomogeneous with degrees of ellipticity for  $P$  and  $S$ -I particle motion dependent on angle of incidence and  $Q^{-1}$  structure.

#### ACKNOWLEDGMENTS

The broadband, high resolution recordings interpreted herein are the result of long-term contributions by a number of colleagues concerned with development of improvements in recording technology, sensor design and emplacement, and computer resources for data analysis. In particular, we appreciate the conscientious efforts of D. Myren in maintaining the site and acquiring the field tapes, A. Linde, S. Sacks, and D. Evertson regarding contributions to strain detection technology, G. Maxwell, G. Jenson, J. Van Schaack and coauthors regarding contributions to the development of GEOS, J. Sena for his important contributions to GEOS maintenance, E. Cranswick and C. Mueller for contributions to software development for data processing, and L. Baker, J. Fletcher, and H. Bundock concerning the capabilities of the computer center. The review comments of J. Andrews, A. McGarr, J. Snoke, and associate editor C. Langston are appreciated. C. Sullivan efficiently and pleasantly turned drafts into decipherable text via TEX.

#### REFERENCES

- Agnew, D. C. (1986). Strainmeters and tiltmeters, *Rev. Geophys. Space Phys.* **24**, 579–624.
- Aki, K. and P. Richards (1980). *Quantitative Seismology: Theory and Methods*, W. H. Freeman, San Francisco, 932 pp.
- Benioff, H. (1935). A linear strain seismograph, *Bull. Seism. Soc. Am.* **25**, 283–309.
- Benioff, H. and B. Gutenberg (1952). The response of strain and pendulum seismographs to surface waves, *Bull. Seism. Soc. Am.* **43**, 229–237.
- Ben-Menahem, A. and S. J. Singh (1981). *Seismic Waves and Sources*, Springer-Verlag, New York, 1108 pp.
- Borcherdt, R. D. (1973). Energy and plane waves in linear viscoelastic media, *J. Geophys. Res.* **78**, 2442–2453.
- Borcherdt, R. D. (1977). Reflection and refraction type-II  $S$  waves in elastic and anelastic media, *Bull. Seism. Soc. Am.* **67**, 43–67.
- Borcherdt, R. D. (1982). Reflection-refraction of general  $P$  and type-I  $S$  waves in elastic and anelastic solids, *Geophys. J. R. Astr. Soc.* **70**, 621–638.
- Borcherdt, R. D. (1988). Volumetric strain in relation to particle displacements for body and surface waves in a general viscoelastic half-space, *Geophys. J. R. Astr. Soc.* **93**, 215–228.
- Borcherdt, R. D., J. B. Fletcher, E. G. Jensen, G. L. Maxwell, J. R. Van Schaack, R. E. Warrick, E. Cranswick, M. J. S. Johnston, and R. McClearn (1985). A general earthquake observation system (GEOS), *Bull. Seism. Soc. Am.* **75**, 1783–1826.

- Borcherdt, R. D. and G. Glassmoyer (1989). An exact anelastic model for the free-surface reflection of  $P$  and  $S$ -I waves as detected by volumetric strain meters and seismometers, *Bull. Seism. Soc. Am.* **79** (in press).
- Borcherdt, R. D., G. Glassmoyer, and L. Wennerberg (1986). Influence of welded boundaries in anelastic media on energy flow and characteristics of  $P$ ,  $S$ -I, and  $S$ -II waves: observational evidence for inhomogeneous body waves in low-loss fluids, *J. Geophys. Res.* **91**, 11503–11,518.
- Borcherdt, R. D. and L. Wennerberg (1985). General  $P$ , type-I  $S$ , and type-II  $S$  waves in anelastic solids: inhomogeneous wave fields in low-loss solids, *Bull. Seism. Soc. Am.* **75**, 1729–1763.
- Crampin, S. (1984). An introduction to wave propagation in anisotropic media, *Geophys. J. R. Astr. Soc.* **76**, 17–28.
- Crampin, S., R. A. Stephen, and R. McGonigle (1982). The polarization of  $P$  waves in anisotropic media, *Geophys. J. R. Astr. Soc.* **68**, 477–485.
- Cranswick, E. and C. Dietel (1985). DSDMAP: a digital seismic data management package, Computer software documentation, U.S. Geol. Surv. Admin. Rep..
- Crossley (1987). RAYAMP-PC version 2.0, Geophysics Lab, McGill University, Montreal, Canada, 9 pp.
- Evertson, D. W. (1977). Borehole strainmeters for seismology, Rep. ARL-TR-77-62, Applied Research Lab., University of Texas, Austin, Texas.
- Gupta, I. N. (1966). Response of a vertical strain seismometer to body waves, *Bull. Seism. Soc. Am.* **56**, 785–791.
- Hadley, D. and H. Kanamori (1978). Seismic structure of the Transverse ranges, California, *Bull. Geol. Soc. Am.* **88**, 1469–1478.
- Johnston, M. J. S. and R. D. Borcherdt (1984). Earth strain in the period range 0.1–10,000 seconds at six borehole sites within the San Andreas fault system, *EOS* **65**, 1015.
- Johnston, M. J. S., Borcherdt, R. D., Gladwin, M. T., Glassmoyer, G., and Linde, A. T. (1987b). Static and dynamic strain during the  $M_L$  5.9 Banning, California, earthquake on July 8, 1986, *EOS* **68**, 1244.
- Johnston, M. J. S., R. D. Borcherdt, and A. T. Linde (1986). Short-period strain ( $0.1$ – $10^5$  s): near-source strain field for an earthquake ( $M_L$  3.2) near San Juan Bautista, California, *J. Geophys. Res.* **91**, 11,497–11,502.
- Johnston, M. J. S., A. T. Linde, M. T. Gladwin, and R. D. Borcherdt (1987 a), Fault failure with moderate earthquakes, *Tectonophysics* **144**, 189–206.
- Johnston, M. J. S., A. T. Linde, I. Sacks, and D. Myren (1982). Borehole dilatometer strain array—Installation and preliminary results from the Mojave desert, *EOS* **63**, 430.
- Jones, L. M., L. K. Hutton, D. D. Given, and C. R. Allen (1986). The North Palm Springs, California earthquake sequence of July, 1986, *Bull. Seism. Soc. Am.* **76**, 1830–1837.
- McDonal, F. J., F. A. Angona, R. L. Mills, R. L. Sengush, R. G. van Nostrand, and J. E. White (1958). Attenuation of shear waves and compressional waves in Pierre shale, *Geophysics* **23**, 421–439.
- McGarr, A., I. S. Sacks, A. T. Linde, S. M. Spottiswoode, and R. W. Green (1982). Coseismic and other short-term strain changes recorded with Sacks-Evertson strain meters in a deep mine, *Geophys. J. R. Astr. Soc.* **70**, 717–740.
- Mediguren, J. A. (1969). Study of focal mechanism of deep earthquakes in Argentina using non-linear particle motions of  $S$  waves, *Bull. Seism. Soc. Am.* **59**, 1449–1473.
- Nuttli, O. (1961). The effect of the Earth's surface on the  $S$  wave particle motion, *Bull. Seism. Soc. Am.* **51**, 237–246.
- Peacock, S., S. Crampin, D. Booth, and J. B. Fletcher (1988). Shear wave splitting in the Anza seismic gap, southern California: temporal variations as possible precursors, *J. Geophys. Res.* **93**, 3339–3356.
- Romney, C. (1957). A combined strain-displacement seismograph, SSA Meeting, Los Angeles.
- Romney, C. (1959). Deep hole detection techniques, in *Need for Fundamental Research in Seismology*, U.S. Department of State, Washington, D.C.
- Romney, C. (1964). Combinations of strain and pendulum seismographs for increasing the detectability of  $P$ , *Bull. Seism. Soc. Am.* **54**, 2165–2174.
- Sacks, I. S. (1979). Borehole strain meters, Proc. of the Conference on Stress and Strain Measurements Related to Earthquake Prediction, *U.S. Geol. Surv., Open-File Rept. 79-370*, 425–485.
- Sacks, I. S., J. A. Snoke, R. Evans, G. King, and J. Beavan (1976). Single-site phase velocity measurements, *Geophys. J. R. Astr. Soc.* **46**, 253–258.
- Sacks, I. S., S. Suyehiro, D. W. Evertson, and Y. Yamagishi (1971). Sacks-Evertson strain meter, its installation in Japan and some preliminary results concerning strain steps, *Pap. Meteorol. Geophys.* **22**, 195–207.
- Sacks, I. S., S. Suyehiro, A. T. Linde, and S. A. Snoke (1978). Slow earthquakes and stress redistribution, *Nature* **275**, 599–602.

- Silverman, S., C. Mortensen, and M. Johnston (1988). A satellite based digital data system for low-frequency geophysical data, *Bull. Seism. Soc. Am.* **79** (in press).
- Snoke, J. A., A. T. Linde, and I. S. Sacks (1981). Seismic moment determinations for nearby earthquakes, *Carnegie Inst. Wash. Year Book* **80**, 493-499.
- Spence, G. D., K. P. Whittall, and R. M. Clowes (1984). Practical synthetic seismograms for laterally varying media calculated by asymptotic ray theory, *Bull. Seism. Soc. Am.* **74**, 1209-1223.
- Suyehiro, S. (1982). Continuous observation of crustal movement, in *Earthquake Prediction Techniques: Their Applications in Japan*, T. Asada, Editor, Columbia University Press, New York, 133-174.
- Wyatt, F. and D. Agnew (1982). Strain and tilt offsets from an earthquake in southern California, *EOS* **63**, 375.

U.S. GEOLOGICAL SURVEY  
345 MIDDLEFIELD ROAD  
MENLO PARK, CALIFORNIA 94025

Manuscript received 2 November 1988